Journal of Nano- and Electronic Physics
Vol. **13** No 5, 05007(9pp) (2021)

Журнал нано- та електронної фізики
Том **13** № 5, 05007(9cc) (2021)

Spatial Distributions of $3p^54s$ States of Argon Atoms in RF Magnetron Sputtering Plasma with a Collisional-Radiative Model

M. Azzaoui[1,2,*], F. Khelfaoui[3], Z. Ballah[3,4]

[1] *Univ. Ouargla, Fac. Des Mathématiques et des Sciences de la Matière, Ouargla 30000, Algeria*
[2] *Laboratoire des Materiaux, Technologie des Systemes Energetiques et Environnement, Faculté des Sciences et Technologie, Université de Ghardaia, Ghardaia 47000, Algeria*
[3] *Univ. Ouargla, Fac. Des Mathématiques et des Sciences de la Matière, Lab. Rayonnement et Plasmas et Physique des Surfaces, Ouargla 30000, Algeria*
[4] *Univ. Ouargla, Fac. des Sciences Appliquées, Ouargla 30000, Algeria*

(Received 16 June 2021; revised manuscript received 20 October 2021; published online 25 October 2021)

Thin films are used in various industrial fields, namely in the manufacture of solar cells, flat screens and in improving the physical properties of material surfaces. In thin film deposition processes, the degree of equilibrium and other plasma characteristics such as the nature, density and temperature must be identified in order to understand the occurrence of various phenomena. In this work, the main focus is on studying the spatial distributions of densities of excited states of Ar* (3p54s ($1s_x$: x = 2-5)), as well as the relative contributions of processes such as the electron impact effect, the radiative de-excitation, the diffusion phenomena of metastable states and the Penning ionization in the population and depopulation of different argon atoms states. For this purpose, a Collisional-Radiative Model (CRM) including 41 states was applied using specified parameters in RF magnetron sputtering plasma. These parameters include electron temperature, electron and ion densities of argon. The rate equations of the state densities led to a matrix system that was solved numerically by iterative Gauss-Seidel Method. The results show that the axial distributions of different excited states and those on the cathode side are slightly larger than those found on the anode side, and they show also that both densities are less than at the reactor center. For metastable states 3p54s (1s5, 1s3), the Penning ionization is important, but it is not important for resonant states 3p54s (1s4, 1s2). Different densities of the excited states are not symmetrical with respect to the center of the reactor due to the existence of a magnetic field at the cathode.

Keywords: Collisional-radiative model, RF magnetron sputtering, Penning ionization, Diffusion phenomena.

DOI: 10.21272/jnep.13(5).05007 PACS number: 66.30.hk

1. INTRODUCTION

In many laboratories, magnetron sputtering systems are the most used process for thin film deposition in advanced industry applications like microelectronics, semiconductors and nanofabrication. These systems usually consist of a cathode through which electromagnetic power is supplied to the reactor that is filled with an inert gas like argon [1]. RF magnetron sputtering plasma has been the subject of many studies by analytical theories and numerical models using experimental techniques [1-5]. Plasma in these devices is typically not in a state of Local Thermodynamic Equilibrium (LTE) [6].

Collisional-Radiative Models (CRMs) are used to investigate and simulate the collisional and radiative processes in plasma in non-LTE condition as reported in many research papers. X.M. Zhu et al. [7] proposed a simple CRM of low pressure argon discharges. A. Bultel et al. [8] studied the influence of Ar_2^+ in an argon CRM. In the work of Zhu-Wen Cheng et al. [9], electron impact excitation rate coefficient from argon $3p^54s$ states to $3p^55p$ states was measured. However, this model is very simplified, since it lumps argon neutral excited states into only 4 effective energy states [10]. Another CRM, by Yanguas-Gil et al., takes into account not only electron impact collisions, but also inelastic collisions induced by argon atoms [10]. There have been several previous attempts to develop a CRM for argon plasma in order to study the excited state of argon under conditions of RF magnetron sputtering. A. Palmero et al. [1] developed a simple CRM for magnetron sputtering argon plasma, which included 12 effective energy states, and studied the behavior of the excited states.

This study is interested in investigating the spatial densities of excited states, as well as the relative contributions of the population and depopulation processes of different states of argon atoms in order to understand the kinetics of plasma in RF magnetron sputtering discharges.

2. THEORETICAL FOUNDATIONS AND NUMERICAL MODEL

2.1 Fundamentals of CRM

In a CRM, state (or level) is used to denote a particular member of the population vector **N** [11]. The balance equation of state i is given by

$$\frac{dN_i}{dt} = R_{prod,i} - R_{loss,i}. \quad (1)$$

The diffusion of states to the walls was treated as the first order process with a rate coefficient v_i^D.

*mohazzaoui@gmail.com

 © 2021 Sumy State University

Equation (1) can be written as:

$$\frac{\partial N_i}{\partial t} + \upsilon_i^D N_i = R_{prod,i} - R_{loss,i}\,, \qquad (2)$$

where N_i is the population density of state i, $R_{prod,i}$ and $R_{loss,i}$ are the rate of production of particles in state i and their loss (consumption), respectively.

In this paper, the elementary processes taken into account are the following:

1. Radiative de-excitation (rad-deex);
2. Radiative recombination (rad-recomb);
3. Electron impact excitation and de-excitation (Excit,e and De-excit,e);
4. Electron impact ionization (ionz,e) and three-body recombination: the third body is an electron (three-body recombination is neglected);
5. Penning ionization of sputtered atoms (PI);
6. Diffusion and subsequent de-excitation at the walls (D).

2.2 Numerical Model

Taking into account different elementary processes mentioned above, the rate equations in steady state ($\partial N_i/\partial t = 0$) can be written as:

$$\upsilon_i^D N_i = R_{prod,i} - R_{loss,i}\,,$$

$$R_{prod,i} = n_e \sum_j X_{ij} N_j + \sum_{j<i} A_{ij} N_j + n_e R_{rad,i} N^+\,, \qquad (3)$$

$$R_{\mathrm{loss},i} = n_e \sum_j X_{ji} N_i + \sum_{j<i} A_{ji}^{eff} N_i + n_e S_i N_i + \\ + (k_{PI} N_{Zn} + \upsilon_i^D) N_i \delta_{im}$$

The resulting system is a combination of $(Nt-1)$ equations, which can be written in a matrix form:

$$C.N = B\,, \qquad (4)$$

C is a square matrix of dimensions $(Nt-1)\times(Nt-1)$, N and B are the vectors of $(Nt-1)$ components,

$$C = \begin{pmatrix} C_{2,2} & n_e X_{2,3} + A_{2,3}^{eff} & \dots & n_e X_{2,\mathrm{Nt}} + A_{2,\mathrm{Nt}}^{eff} \\ n_e X_{3,2} & C_{3,3} & \dots & n_e X_{3,\mathrm{Nt}} + A_{3,\mathrm{Nt}}^{eff} \\ \vdots & \vdots & \ddots & \vdots \\ n_e X_{\mathrm{Nt},2} & n_e X_{\mathrm{Nt},3} & \dots & C_{Nt,Nt} \end{pmatrix} \qquad (5)$$

There are $(Nt-1)$ unknown quantities ($Nt-1$ densities of sates) in Eq. (4). It becomes a linear system of equations which could be easily solved using the numerical Gauss-Seidel iterative algorithm. C_{ij} are coefficients which combine the rates of some processes. For $i = 2, 3, ..., Nt$, the coefficients C_{ii} take the following expression:

$$C_{i,i} = -n_e\left(\sum_{j\neq i} X_{i,j} + S_i\right) - \sum_{j=1}^{i-1} A_{i,j}^{eff} - (k_{PI} N_{Zn} + \upsilon_i^D)\delta_{im}\,, \qquad (6)$$

where δ_{im} is the Kronecker function symbol and $m = 2$ or 4, N^+ is the density of argon ions, X_{ij} is the rate coefficient for electron impact excitation/de-excitation from state i to state j, S_i is the rate coefficient for electron impact ionization, k_{PI} is the rate coefficient for Penning ionization, $R_{rad,i}$ is the rate coefficient of radiative recombination.

The effective transition probability $A_{i,j}^{eff}$ is given by

$$A_{i,j}^{eff} = \Lambda_{i,j} A_{i,j}\,, \qquad (7)$$

where $A_{i,j}$ is the radiative transition probability from state i to state j, $\Lambda_{i,j}$ is the optical escape factor for the transition, which takes into account that an emitted photon can be reabsorbed by plasma via self-absorption [12].

The vector B is determined as

$$B = -\begin{pmatrix} B_2 \\ B_3 \\ \vdots \\ B_{Nt} \end{pmatrix}, \qquad (8)$$

where B_i is defined in the following form:

$$B_i = -n_e R_{rad,i} N^+ - n_e X_{i,1} N_1\,. \qquad (9)$$

An argon CRM predicts the population densities of particles in different states with the need of some parameters such as electron temperature, electron and ion densities and density of argon atoms in the plasma (pressure and temperature of the neutral gas). The average values of electron and ion densities, as well as the electron temperature calculated by Ballah et al. [13, 14], were used to apply the CRM in RF magnetron sputtering. Fig. 1 shows the RF magnetron discharge geometry [13].

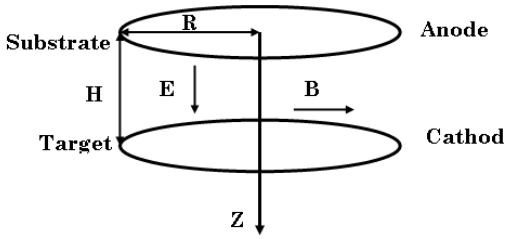

Fig. 1 – Scheme of the magnetron discharge geometry [13]

Let H be the distance between electrodes and let R be the radius of each electrode; we also assume that R is much greater than H. The anode is located at $z \sim 0$ cm and the cathode is located at $z \sim H = 3$ cm. The sputtering reactor is alimented by RF voltage with a frequency $f_{RF} = 13.56$ MHz, the voltage difference is 100 V and the magnetic field B at the cathode is 30 Gauss. The parameters of the RF magnetron sputtering plasma are a function of the position (z) and time (t). The averages of electron and ion densities, electron temperature and electric field are calculated over a period $T = 2\pi / f_{RF}$ (Fig. 2).

The initial density of neutral Ar atoms N_1 can be evaluated approximately through the ideal gas law $N_1 \approx N_0 = p_g / k_B T_g$. For boundary conditions, $z = 0$ and $z = H$, the change in the densities near the surface is considered slow, therefore $dN_i/dz = 0$. The general scheme used in the CRM for calculating the state densities is as follows:

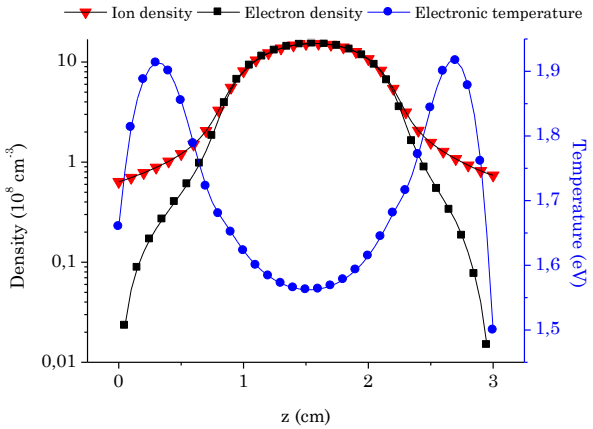

Fig. 2 – Average densities of argon ions and electrons and average electron temperature in 13.56 MHz RF discharge

– Step 1: Reading the electron and ion densities, as well as the electron temperature, and then calculating the reaction rate coefficients required for the model;
– Step 2: Initialization of the densities of all states N_i and all space steps along the z axis of the cylinder;
– Step 3: Running of the calculation for each z value of the system of equations (4) by iterative Gauss-Seidel method.
– Step 4: Testing the convergence of the solution for all states i and all steps of position z.
– Step 5: End of calculation if the solution of density converges; otherwise, return to step 3 and repeat.

3. ATOMIC DATA AND PLASMA PARAMETERS

3.1 Atomic State System

The atomic state system used in our numerical model is formed of 41 argon atom states, including the ground state (GS: $3p^6(^1S_0)$, argon ions in the ground state ($3p^5$), electrons (e^-) and the sputtered atom in the ground state (Zn, for example). Indeed, the states are divided into two subsystems with two different ionization limits: the first core configuration ($j_c = 3/2$), also called the "nonprimed" subsystem, has an ionization limit $E_{ionz} = 15.760$ eV, and the second one ($j_c = 1/2$), called the "primed" subsystem, $E_{ionz} = 15.937$ eV [8]. The argon energy states, radiative transition probabilities, state degeneracy used in our calculation are obtained from the NIST database [15] and from [16]. Paschen's notation is adopted as state notation here. In Paschen's notation, the first four levels excited are labeled as $1s_5$ to $1s_2$, where $1s_5$: $3p^5 4s$ ($^3P_2$) and $1s_3$: $3p^5 4s$ ($^3P_0$) for the two metastable levels and $1s_4$: $3p^5 4s$ ($^3P_1$) and $1s_2$: $3p^5 4s$ ($^1P_1$) for the two resonance levels. Likewise, the ten levels of the $3p^5 4p$ configuration are labeled as $2p_{10}$ to $2p_1$.

3.2 Rate Coefficients of Processes

The main Ar atomic transitions considered in this study are:

$$3d, 5s, 4s \rightleftarrows 3p^6$$
$$4p, 5p \rightleftarrows 4s$$
$$5s \rightleftarrows 4p$$
$$4p, 5p \rightleftarrows 3d$$
$$Ar \rightleftarrows Ar^+$$

These electronic transitions are related to a set of processes R that is characterized by the rate coefficients, which are mostly related to the electron temperature. The rate coefficient is related to the cross section by:

$$X_R = \int_0^\infty \sqrt{\frac{2E}{m_e}} \sigma_R(E) f(E) dE \,, \qquad (10)$$

where R denotes the considered processes, σ_R is the cross section of the processes R, X_R is the rate coefficient of the processes R, E is the energy of incident electrons, $f(E)$ is the Electron Energy Distribution Function (EEDF) which is assumed in this study as Maxwellian. The rate coefficients X_R can be calculated with a numerical program for each process. These transitions are classified, according to the selection rules, into two categories: allowed transitions and forbidden transitions (parity forbidden, spin forbidden). Transitions between subsystem $J_c = 3/2 \rightarrow J_c = 1/2$ are also forbidden in the case of collisional transitions.

The cross sections for electron impact excitation between the states are taken as:

$$\sigma_{excit,e}(i,j,E) = \sigma^A(i,j,E) + \sigma^{PF}(i,j,E) + \sigma^{SF}(i,j,E) \,, \quad (11)$$

where i and j denote the lower and upper states, respectively, E is the incident electron energy,
• σ^A symbolizes the cross sections for optically allowed transitions ($\Delta l = \pm 1$, $\Delta J = 0, \pm 1$, but not $J = 0 \rightarrow J = 0$). The cross sections of these allowed transitions are of the form $\sigma^A \sim a(E/E_{ji}) \ln(bE/E_{ji})$, where E_{ij} is the energy difference between level j and level i ($E_{ji} = E_j - E_i$),
• σ^{PF} symbolizes the cross sections for parity forbidden transitions ($\Delta l \neq \pm 1$), σ^{SF} symbolizes the cross sections for spin forbidden transitions ($\Delta l = \pm 1$; $\Delta s \neq 0$; $\Delta J \neq 0 \pm 1$, including $J = 0 \rightarrow J = 0$). The cross sections of these two types of forbidden transitions have the form $\sigma \sim a(E - E_{ji})^b / E$, where $E - E_{ji}$ is the energy of an electron after collision. It is assumed that the forbidden transitions are only considered between the ground state and the first four excited states.

The cross sections for electron impact de-excitation are obtained from the corresponding cross sections for electron impact excitation based on the principle of detailed balance:

$$\sigma_{de-excit,e}(i,j,E') = \frac{g_i}{g_j} \frac{E}{E'} \sigma_{excit,e}(i,j,E) \,, \qquad (12)$$

where $E' = E - E_{ji}$, g_i and g_j are the state degeneracies of the lower and upper states, respectively.

With a numerical program, collisional cross sections are calculated for each energy state as a function of electron energy using parameters and formulas found in literature [17].

The cross sections for electron impact ionization can be written in the form [8]:

$$\sigma_{ionz,e} = 4\pi a_0^2 \left(E_1^H / E_{ionz}(i)\right)^2 \alpha_i \left(U(i)\right)^{-2} \times \left(U(i)-1\right) \ln\left(1.25\beta_i U(i)\right) \quad (13)$$

where $U(i) = E/E_{ionz}(i)$, α_i and β_i are the parameters depending on states.

Using the principle of detailed balance, the cross section of radiative recombination was estimated from the corresponding cross section of photoionization taken under equilibrium conditions as presented in the work of Boffard [16].

For sputtered Zn atoms, the rate coefficient of Penning ionization is $k_{PI} = 1.7\times10^{-7}$ cm^3/s.

An additional process is transport diffusion and subsequent de-excitation on the walls. The probability of quenching per unit time of this process is taken into account in the following way [18]:

$$\upsilon_i^D = D_i / \Lambda^2 , \quad (14)$$

This term (Eq. (14)) is only important for the metastable states. For other states, it can be neglected with respect to collisional and radiative processes. Diffusion coefficients of Ar metastable states under standard conditions (T_0 = 300 K) are as follows:

$$Dn_{1s5} = 1.8\times10^{18}\ \text{cm}^{-1}\text{s}^{-1},$$
$$Dn_{1s3} = 1.9\times10^{18}\ \text{cm}^{-1}\text{s}^{-1},$$

where Dn_i is the diffusion coefficient multiplied by gas density, and index denotes the atom state. Taking into account the dependence of Dn_i on temperature, the diffusion coefficient D_i can be expressed as [18]:

$$D_i = \frac{Dn_i}{n_g}\sqrt{\frac{T_g}{T_0}}, \quad (15)$$

In our case, the radius of the electrode is much greater than the distance between electrodes, so $\Lambda = H/\pi$ where Λ is the diffusion length for this geometry.

3.3 Characteristic Time of Some Processes

The following formulas show the characteristic time of some processes included in our model.

– The characteristic time depends on electron impact excitation and de-excitation from state i to all other states:

$$\tau_i^{col,e} = 1/\left(n_e \sum_{j=1,(i\neq j)} X_{ij}\right).$$

– The characteristic time depends on radiative de-excitation of state i towards all the lower states:

$$\tau_i^{Rad-deex} = 1/\left(\sum_{transitions} A_{ji}^{eff}\right).$$

– The characteristic time depends on electron impact ionization of state i:

$$\tau_i^{\text{ionz},e} = 1/\left(n_e S_i\right).$$

– The characteristic time depends on collisional ionization by sputtered atoms M (Penning ionization) of state i:

$$\tau_i^{PI} = 1/\left(k_{PI} N_M\right).$$

– The characteristic time of metastable diffusion is:

$$\tau_i^D \approx 1/\left(D_i / \Lambda^2\right).$$

4. RESULTS AND DISCUSSION

Determination of the plasma parameters is an important subject, mainly in its design and analysis.

4.1 Cross Section of Excitation and De-excitation Processes

Fig. 3a, Fig. 3b and Fig. 3c show the typical curves of the cross section (σ) for electron impact collisions. Fig. 3a presents ionization cross sections from the ground state and from $1s_5$ state. Fig. 3b and Fig. 3c present the excitation cross sections between (GS – $1s_x$: x = 2 – 5), (GS – $2p_{10}$) and (GS – $2p_4$) and some examples of cross sections for electron impact excitation used in our mode. The transitions between the ground state and resonant states $3p^54s$ ($1s_4$, $1s_2$) are allowed, those between ground states and metastable states $3p^54s$ ($1s_5$, $1s_3$) are spin forbidden and those between ground states and states $3p^54p$ ($2p_{10}$, $2p_4$) are parity forbidden transitions.

As it can be seen, the cross section shows a rapid increase at low electron incident energy (about 15 eV for metastable states and about 30 eV for resonant states) followed by a decrease at higher energy. Because of their spin-changing nature, cross sections for direct excitation from the ground state to $3p^54s$ ($1s_3$) or $3p^54s$ ($1s_5$) states show a peak at an energy above the threshold (energy difference E_{ji}) and a rapid decrease with increasing incident electron energy. Cross sections for electron impact excitation from the ground state to resonant states $3p^54s$ ($1s_4$, $1s_2$) are greater than those found in excitation to metastable states $3p^54s$ ($1s_5$, $1s_3$). In addition, cross sections for electron impact excitation

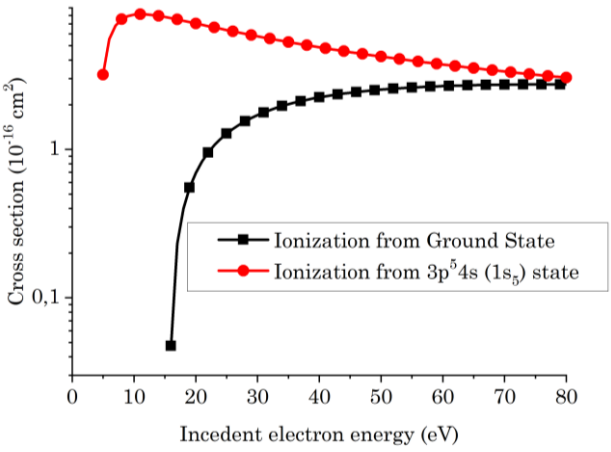

Fig. 3a – Ionization cross section from the ground state and $3p^54s$ ($1s_5$) state

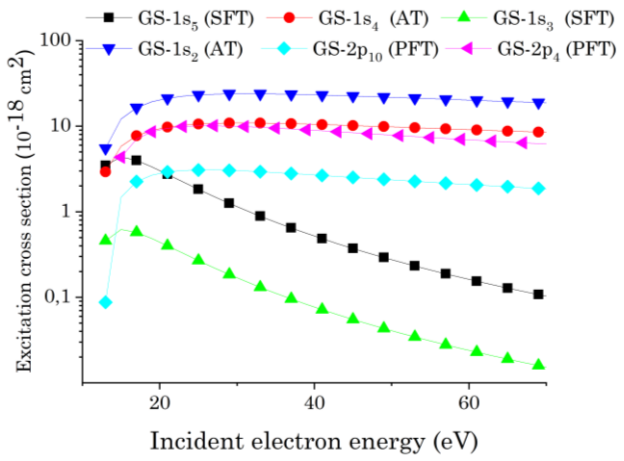

Fig. 3b – Excitation cross section from the ground state to some higher states

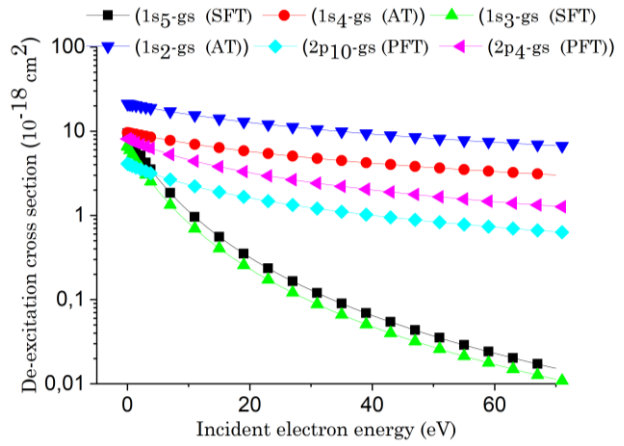

Fig. 3c – De-excitation cross section from some higher states to the ground state* (AT: allowed transition; PFT: parity forbidden transition, SFT: spin forbidden transition)

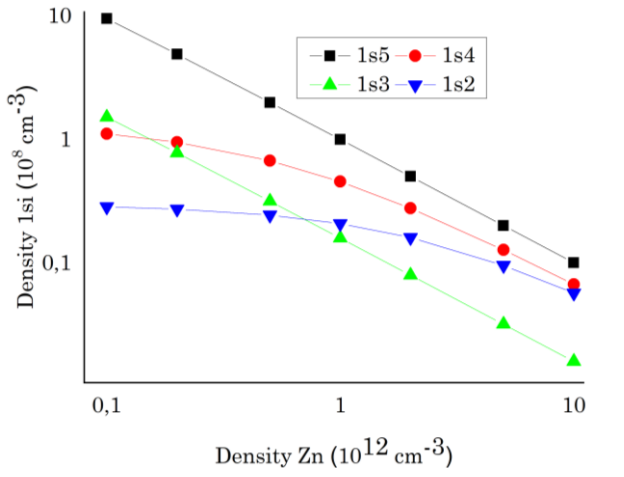

Fig. 4 – Density of neutral argon in $1s_x$ state as a function of sputtered Zn

from the ground state to states $3p^54p$ ($2p_{10}$ and $2p_4$) are greater than those found in excitation to metastable states $3p^54s$ ($1s_5$, $1s_3$). It is also clear that the highest cross section for electron impact excitation occurs upon excitation from the ground state to resonant states $3p^54s$ ($1s_4$, $1s_2$).

As seen in Fig. 3c, the collisional de-excitation cross section shows a decrease with respect to incident electron energy lower than the peak energy in contrary to the excitation cross section. At higher incident energy, both cases (excitation and de-excitation cross sections) show a similar trend of decrease.

4.2 Penning Ionization Processes

Currently, the focus is on collisions between argon atoms in metastable states $3p^54s$ ($1s_5$, $1s_3$) and sputtered Zn atoms ($Ar\ (^3P_{2,0}) + Zn \rightarrow Ar + Zn^+ + e^-$). Variations of population of excited states $3p^54s$ are calculated, taking into account Penning ionization, as a function of the density of Zn in the plasma. We notice that the densities of excited states $3p^54s$ decrease when the density of sputtered Zn atoms increases (Fig. 4). This behavior is logical, because the energy stored in atoms in $3p^54s$ states (> 11 eV) is greater than the ionization potential of Zn atoms (9.4 eV).

4.3 Characteristic Time and Choice of Dominant Processes

In most argon plasmas, $3p^54s$ states are very interesting, since they are generally more populated than higher excited states; therefore, they serve as a source of energy for chemical reactions. These states represent a considerable factor in plasma kinetics and energy transfer processes.

Table 1 shows the characteristic time of electron impact excitation/de-excitation $\tau_i^{col,e}$, radiative de-excitation $\tau_i^{Rad-deex}$ and electron impact ionization $\tau_i^{\text{ionz},e}$ of state i.

Table 1 – Characteristic times for the first four excited states

	$1s_5$	$1s_4$	$1s_3$	$1s_2$
$\tau_i^{col,e}$ (s)	1.9×10^{-4}	3.3×10^{-4}	1.3×10^{-3}	1.39×10^{-4}
$\tau_i^{Rad-deex}$ (s)	56*	4.69×10^{-6}	45*	3.58×10^{-6}
$\tau_i^{\text{ionz},e}$ (s)	7.93×10^{-4}	1.26×10^{-3}	3.97×10^{-3}	1.24×10^{-3}

*These high periods are a characteristic of metastable states

Diffusion characteristic times for $1s_5$ and $1s_3$ are, respectively, $\tau_i^D = 1.63\times10^{-3}$ s and $\tau_i^D = 1.54\times10^{-3}$ s. Characteristic times for Penning ionization processes $\tau_i^{PI} = 5.88\times10^{-5}$ s at Zn density of ~ 10^{11} cm^{-3}.

It is noticed that

– for all $3p^54s$ states $\tau_i^D << \tau_i^{col,e}, \tau_i^{ionz,e}$,

– for metastable states $\tau_i^D, \tau_i^{PI} << \tau_i^{rad-deex}$ and $\tau_i^{PI} << \tau_i^D$,

– for resonant states $\tau_i^{rad-deex} << \tau_i^D, \tau_i^{PI}, \tau_i^{col,e}, \tau_i^{ionz,e}$.

Penning ionization process of sputtered particles by metastable states is a very important loss process because $\tau_i^{PI} << \tau_i^D, \tau_i^{ionz,e}, \tau_i^{col,e}, \tau_i^{rad-deex}$ but for resonant states it is less important process because $\tau_i^{rad-deex} << \tau_i^{PI}$. It is clear that the existence of a sputtered Zn atom changes plasma kinetics.

Electron impact and radiative processes were the only processes taken into account for higher excited states ($4p$, $3d$, $5s$, $5p$, …).

4.4 Spatial Distributions of Rate Coefficients of Collisional Processes

The axial structure of the calculated plasma properties is similar to the rate coefficients most evident in the profiles generated by the CRM.

4.4.1 Rate Coefficients of Electron Impact Excitation

Fig. 5 presents the rate coefficient of electron impact excitation from the ground state to some higher states.

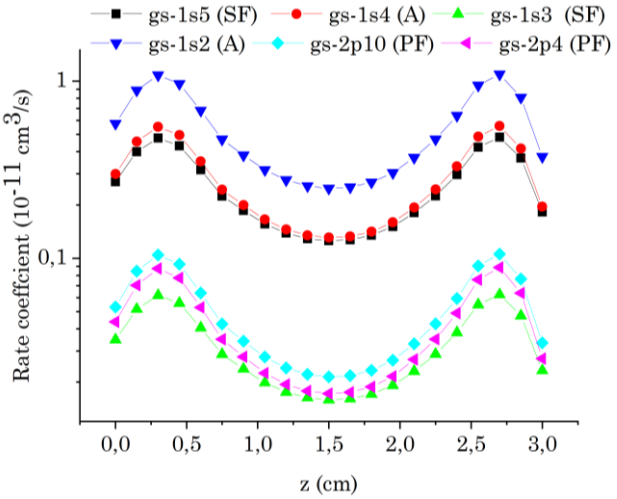

Fig. 5 – Rate coefficient of electron impact excitation from the ground state to some higher states

The excitation rate coefficient profiles present a substantial variation in the plasma. According to the z position, the excitation rate coefficients (X_{ij}) are minimum at the reactor center. Two peaks of the rate coefficients move away from the electrodes and are immersed in the plasma sheath. While the rate coefficients have minimum values at the reactor center, near the anode and cathode these values increase.

We can see the rate coefficients of electron impact excitation for $1s_x$ states, corresponding to parity forbidden transition, at the reactor center ($n_e = 1.5\times10^9$ cm^{-3}, $p = 13.33$ Pa and $T_e = 1.56$ eV). The rate coefficient of electron impact excitation is about 10^{-9} to 10^{-7} cm^{-3}/s. The value of the rate coefficient from the metastable state $1s_5$ towards resonant states $1s_4$ is 2.04×10^{-7} cm^{-3}/s and its value from resonant states $1s_4$ towards resonant states $1s_2$ is 1.11×10^{-8} cm^{-3}/s, while its value from the metastable state $1s_5$ towards the metastable state $1s_3$ is 6.39×10^{-9} cm^{-3}/s.

For electron impact de-excitation between four $1s$ states, the rate coefficients are almost constant in different z positions of the reactor.

4.4.2. Rate Coefficients of Ionization and Recombination Processes

According to the z position, the rate coefficients of electron impact ionization S_i vary depending on the electron temperature (Fig. 6).

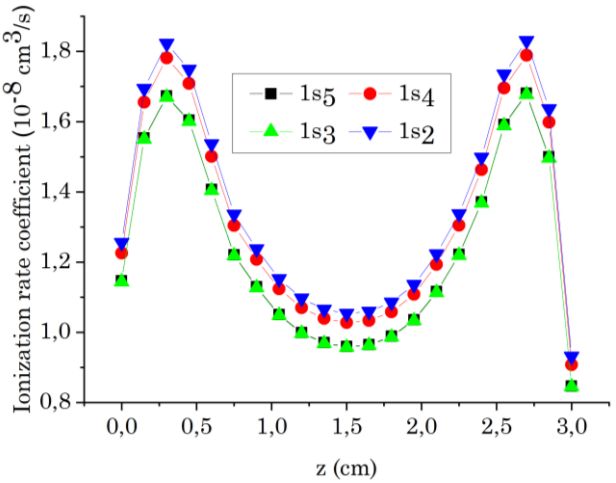

Fig. 6 – Profiles of ionization rate coefficients of atoms from $3p^54s$ ($1s_x$) states

It is observed that the ionization rate coefficients from excited states (~ 10^{-8} cm^{-3}/s) are more important than the ionization rate coefficient from the ground state by direct ionization ($S_1 = 1.3\times10^{-12}$ cm^{-3}/s at the reactor center). In radiative recombination, the rate coefficients are almost constant for different z positions in the reactor. The rate coefficient of radiative recombination to the fundamental state ($R_{rad,1} = 9.8\times10^{-14}$ cm^{-3}/s) is more important than those to excited states (~ 10^{-16} cm^{-3}/s for $3p^54s$ states).

4.5 Spatial Densities of Excited States and Relative Contributions of Processes

4.5.1 Densities of States

In the cathode and anode zones, the density of ground states remains constant ($N_1 \approx N_0$) and decreases slightly at the reactor center. Indeed, the density ratios of neutrals to the density of atoms at a metastable level is less than 5×10^{-7}.

According to our findings, 3 different regions can be clearly seen in the profiles of the population of excited states as a function of z. These are two electrode regions and the center of the plasma. The density of metastable states $3p^54s$ ($1s_5$, $1s_3$) at the center of the reactor ($n(1s_5) = 1.49\times10^9$ cm^{-3}, $n(1s_3) = 2.38\times10^8$ cm^{-3}) is greater than the density of both extremities (Fig. 7). At the same time, the metastable densities near the cathode ($n(1s_5) = 1.18\times10^8$ cm^{-3}, $n(1s_3) = 1.9\times10^7$ cm^{-3}) are less than those near the anode ($n(1s_5) = 1.63\times10^8$ cm^{-3}, $n(1s_3) = 2.57\times10^7$ cm^{-3}) (see Fig. 7). So, the densities of excited states are not homogeneous in different z positions of the reactor.

The densities of resonant states $3p^54s$ ($1s_4$, $1s_2$) are relatively weak near the plasma sheath interface ($n(1s_4) = 3.5\times10^7$ cm^{-3}, $n(1s_2) = 7.7\times10^6$ cm^{-3}) compared to the bulk plasma ($n(1s_4) = 1.13\times10^8$ cm^{-3}, $n(1s_2) = 2.54\times10^7$ cm^{-3}) and almost zero near the electrodes. In our calculations, the metastable density of $1s_5$ is greater than that of $1s_3$ and the resonance densi-

ty of $1s_4$ is greater than that of $1s_2$.

The population of $3p^54s$ states is consistent with the data reported by L. Maaloul et al. [5] and by L. Maaloul and L. Stafford [19] in RF magnetron sputtering. For atomic metastable states of Ar, the density of Ar $1s_5$ is of the order of 10^9 cm^{-3} and of Ar $1s_3$ is of the order of 10^8 cm^{-3}; for atomic resonant states of Ar, the densities of Ar $1s_4$ and Ar $1s_2$ are of the order of 10^8 cm^{-3}. The ratio of the densities of atoms in $1s_5$ to the densities of atoms in $1s_3$ was found to be around 6 ± 0.5, which is close to that found in the research papers of L. Maaloul et al. [5, 19] and J.B. Boffard et al. [16].

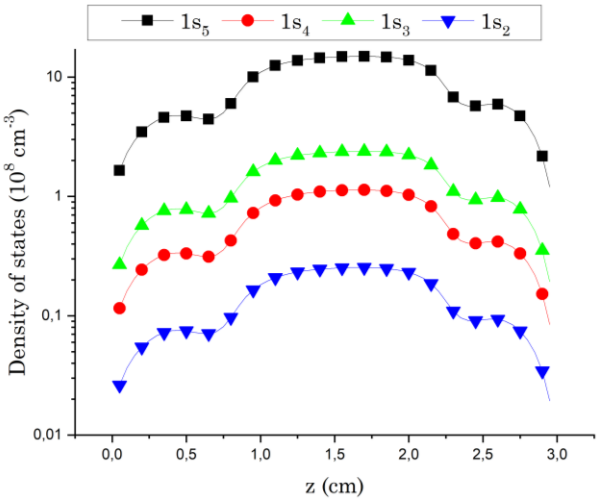

Fig. 7 – Densities of $3p^54s$ ($1s_x$, x = 2, 3, 4, 5) states

4.5.2 Contribution of Production and Loss Mechanism for $3p^54s$ States

In order to estimate the respective contributions of different processes taken into account in our model (Eq. (4)), the population and de-population in metastable and resonant states are presented in Table 2 for $N_{Zn} = 10^{11}$ cm^{-3}. In the production process for each state $1s_x$, we have population by electron impact excitation from the ground state and by electron impact transfers from other near $3p^54s$ states and by radiative de-excitation from high states ($4p$, $3d$, $5s$, $5p$). In the loss process, we have de-population by electron impact excitation to high states ($4p$, $3d$, $5s$, $5p$), by electron impact transfers to the near $3p^54s$ states and by radiative de-excitation to the ground state. The Penning ionization and diffusion are loss process for metastable states.

Table 2 – Relative contributions of some production and loss processes of $3p^54s$ states

	$1s_5$ (N = 2)	$1s_4$ (N = 3)	$1s_3$ (N = 4)	$1s_2$ (N = 5)
Production process				
Excit, e	22.04 %	31.89 %	17.86 %	63.36 %
Rad-deex	77.69 %	65.75 %	81.72 %	36.17 %
Other processes	0.27 %	2.36 %	0.42 %	0.47 %
Loss process				
Eexcit, e	5.1 %	0.23 %	2.97 %	0.31 %
Rad-deex	–	99.42 %	–	99.63 %
PI	89.74 %	–	91.84 %	–
Other processes	5.16 %	0.35 %	5.19 %	0.05 %

In the production process, we include radiative recombination, electron impact de-excitation and electron impact transfers between near $3p^54s$ states in part of other processes. For the loss process, we include electron impact ionization, electron impact de-excitation, electron impact transfers between near $3p^54s$ states for each $1s_x$ and diffusion for metastable states.

In Table 2, we present the relative contributions of the production (population) processes of $3p^54s$. The contribution of electron impact de-excitation via higher states ($4p$, $3d$, $5s$, $5p$) to all $3p^54s$ states is negligible. In the case of metastable states, the contribution of excitation and de-excitation by impact electrons between nearby states is weak $3p^54s$ ($1s_5$, $1s_4$, $1s_3$, $1s_2$), since it is about 0.27 % for level $1s_5$ and 0.41 % for level $1s_3$. Similarly, for resonant states their contribution is about 0.47 % for $1s_2$ and 2.35 % for $1s_4$. The contribution of electron impact excitation via the ground state is important, namely 22.04 % for level $1s_5$, 17.86 % for level $1s_3$, 31.89 % for level $1s_4$ and 63.36 % for level $1s_2$; therefore, this mechanism is main for resonant levels. In addition, the contribution of radiative de-excitation of higher states ($4p$, $5p$, $3d$ etc.) is also important, 77.69 % and 81.72 % for metastable levels $1s_5$ and $1s_3$, 65.75 % and 36.17 % for resonant levels $1s_4$ and $1s_2$.

For the mechanism of loss (depopulation) in $3p^54s$ states, it can be clearly seen that:

– The contribution of electron impact excitation and de-excitation to all states is of the order of 7 % for $1s_5$ and 4 % for $1s_3$.

– Atoms in the metastable state $3p^54s$ ($1s_5$, $1s_3$) will diffuse through the plasma according to the geometry of the discharge chamber. The contribution of the diffusion of metastable atoms to the reactor walls is of the order of 3.24 % for $1s_5$ and 3.50 % for $1s_3$. It is noted that this phenomenon has a weak impact in the range of 100 mTorr.

– The dominant process is the Penning ionization with sputtered Zn atoms, its relative contribution is about 90 % at $N_{Zn} = 10^{11}$ cm^{-3}. The importance of Penning ionization reactions on plasma kinetics during magnetron sputtering with Zn targets illustrated above is in good agreement with the work of L. Maaloul and L. Stafford [19]. Indeed, the authors have shown that in plasmas characterized by relatively low charged particle densities, Penning ionization reactions are the dominant mechanisms for pulverized particles.

– Electron impact ionization and electron impact de-excitation to the ground state are negligible.

5. CONCLUSIONS

CRM methods play a very important role in explaining plasma environment. In this paper, a CRM was applied using parameters of RF magnetron sputtering plasma (electron temperature, electron and ion densities, and argon atom density) in order to determine the excited state population of $1s$ states of argon plasma.

According to our findings, 3 different regions can be distinguished in the profiles of populations of excited states as a function of z: two electrode regions and the center of the plasma.

Densities of excited states $3p^54s$ ($1s_x$: x = 2-5) in different positions increase toward the reactor center; the

state density on the cathode side is greater than that on the anode side, and densities of atoms in the ground state are almost constant. Furthermore, densities of excited states are no longer symmetric with respect to the reactor center because of the existence of a magnetic field B in the target region.

Again, the diffusion phenomenon of metastable atoms changes slightly the distribution of metastable atoms in the sputtering plasma, which increases its density in the center of the reactor and decreases at the limits. However, the effect of diffusion of metastable atoms on the ground state and resonant states distributions is negligible.

The Penning ionization process for metastable states is important ($\tau_i^{PI} < \tau_i^D$ and $\tau_i^{PI} << \tau_i^{ionz,e}, \tau_i^{col,e}, \tau_i^{rad-deex}$), its relative contribution is about 90 % at $N_{Zn} = 10^{11}$ cm^{-3}, but it is not essential for resonant states ($\tau_i^{rad-deex} << \tau_i^{PI}$). These features are reflected in the distribution of atoms in the ground state and atoms in other excited states. An important result obtained from our model consists in identifying populations and estimating the relative contribution of different population and de-population processes in various excited states. The results of this study can be used to control plasma processes, transfer of sputtered atoms and various processes near the plasma substrate interface.

ACKNOWLEDGEMENTS

The authors acknowledge the support of the LRPPS Laboratory of Ouargla University, Algeria, and the Directorate General of Scientific Research and Technological Development (DGRSDT), who supports the Laboratory.

REFERENCES

1. A. Palmero, E. D. Van Hattum, W.M. Arnoldbik, F.H.P.M. Habraken, *J. Surf. Coat. Technol.* **188-189**, 392 (2004).
2. N. Nafarizal, N. Takada, K. Sasaki, *J. Phys. D: Appl. Phys.* **41**, 035206 (2008).
3. J. Kousal, J. Hanuš, A. Choukourov, O. Polonskyi, H. Biederman, D. Slavínská, *Plasma Process. Polym.* **6**, S803 (2009).
4. N. Benchiheb, M.S. Aida, N. Attaf, *Mater. Sci. Eng. B*, **172** No 2, 191 (2010).
5. L. Maaloul, R.K. Gangwar, L. Stafford, *J. Vac. Sci. Technol. A* **30** No 2, 021301 (2012).
6. M. Azzaoui, F. Khelfaoui, *Annales des Sciences et Technologie* **5** No 2, 204 (2013).
7. Z. Xi-Ming, P. Yi-Kang, *J. Phys. Appl. Phys.* **40**, 5202 (2007).
8. A. Bultel, B. Ootegem, A. Bourdon, P. Vervisch, *Phys. Rev.* **E 65**, 046406 (2002).
9. Z.-Wen Cheng, Z. Xi-Ming, S. Nader, G. Xiao-Mi, L. Fei-Xiang, P. Yi-Kang, *J. Phys. D: Appl. Phys.* **48**, 285202 (2015).
10. M. Celik, Experimental, computational studies of electric thruster plasma radiation emission, institution Massachusetts Institute of Technology, PhD thesis (2007).
11. Y. Ralchenko, *Modern methods in collisional-radiative modeling of plasmas*, 90 (Springer: 2016).
12. A. Palmero, E.D. Van Hattum, H. Rudolph, F. Habraken, *J. Appl. Phys.* **101** No 5, 053306 (2007).
13. Z. Ballah, F. Khelfaoui, *J. King Saud Univ.-Sci.* **32** No 1, 620 (2020).
14. Z. Ballah, Interne Communication (2020).
15. *NIST National Institute of Standards and Technology* (2020).
16. J.B. Boffard, B. Chiaro, T. Weber, C.C. Lin, *Atomic Data and Nuclear Data Tables* **93**, 831 (2007).
17. A.M. Keesee, *Neutral density profiles in argon helicon plasmas. PhD thesis* (West Virginia University: 2006).
18. K.E. Evdokimov, M.E. Konischev, V.F. Pichugin, Z. Sun, *Resour.-Effic. Technol.* **3** No 2, 187 (2017).
19. L. Maaloul, L. Stafford, *J. Vac. Soc. A* **31**, No 6, 061306 (2013).

Просторові розподіли станів $3p^54s$ атомів аргону в плазмі високочастотного магнетронного розпилення з радіаційною моделлю зіткнень

M. Azzaoui[1,2], F. Khelfaoui[3], Z. Ballah[3,4]

[1] *Univ. Ouargla, Fac. Des Mathématiques et des Sciences de la Matière, Ouargla 30000, Algeria*
[2] *Laboratoire des Materiaux, Technologie des Systemes Energetiques et Environnement, Faculté des Sciences et Technologie, Université de Ghardaia, Ghardaia 47000, Algeria*
[3] *Univ. Ouargla, Fac. Des Mathématiques et des Sciences de la Matière, Lab. Rayonnement et Plasmas et Physique des Surfaces, Ouargla 30000, Algeria*
[4] *Univ. Ouargla, Fac. des Sciences Appliquées, Ouargla 30000, Algeria*

Тонкі плівки використовуються в різних галузях промисловості, а саме у виробництві сонячних елементів, плоских екранів та для поліпшення фізичних властивостей поверхонь матеріалів. У процесах осадження тонких плівок ступінь рівноваги та інші характеристики плазми, такі як природа, густина і температура, повинні бути визначені, щоб зрозуміти появу різних явищ. У роботі основна увага приділяється вивченню просторових розподілів густин збуджених станів Ar* ($3p^54s$ ($1s_x$: x = 2-5)), а також відносних внесків таких процесів, як бомбардування електронами, випромінювальне дезбудження, явища дифузії метастабільних станів та іонізація Пеннінга в популяції та депопуляції різних станів атомів аргону. Для цього радіаційну модель зіткнень (CRM), яка включала 41 стан, було застосовано з використанням заданих параметрів у плазмі високочастотного магнетронного розпилення. Ці параметри включають температуру електронів, густини електронів та іонів аргону. Кінетичні рівняння густин станів привели до матричної системи, яка була розв'язана чисельно за допомогою

ітераційного методу Гауса-Зейделя. Результати показують, що осьові розподіли різних збуджених станів та станів на катоді трохи більші, ніж на аноді; вони також показують, що обидві густини менші, ніж у центрі реактора. Іонізація Пеннінга важлива для метастабільних станів $3p^54s$ ($1s_5$, $1s_3$), але не важлива для резонансних станів $3p^54s$ ($1s_4$, $1s_2$). Різні густини збуджених станів не є симетричними відносно центру реактора через наявність магнітного поля на катоді.

Ключові слова: Радіаційна модель зіткнень, Високочастотне магнетронне розпилення, Іонізація Пеннінга, Дифузійні явища.